Ligustroflavone protects against acute kidney injury by inhibiting ferroptosis via acting on GSK3β/NRF2 signaling

JIAYU SONG[1,2*], LONG WANG[3*], YARU WANG[1], JIE MENG[4], JINGYI SHENG[2], YONGFENG ZHAO[2], SAN YAN XU[2], JUAN LEI[2], FANGFANG CAI[5] and YUNWEN YANG[1]

[1]Nanjing Key Laboratory of Pediatrics, Children's Hospital of Nanjing Medical University, Nanjing, Jiangsu 210008, P.R. China; [2]Department of Pediatric Nephrology, The Second Affiliated Hospital of Nanjing Medical University, Nanjing, Jiangsu 210003, P.R. China; [3]Department of Cardiology, Translational Medicine Center, Westlake Laboratory of Life Sciences and Biomedicine, Affiliated Hangzhou First People's Hospital, Westlake University School of Medicine, Hangzhou, Zhejiang 310006, P.R. China; [4]Department of Neurology, Jiangsu Key Laboratory of Brain Disease and Bioinformation, Changzhou Wujin People's Hospital, Wujin Clinical College of Xuzhou Medical University, Changzhou, Jiangsu 213017, P.R. China; [5]Department of Cell Biology, School of Basic Medical Sciences, Nanjing Medical University, Nanjing, Jiangsu 211166, P.R. China

Received January 9, 2026; Accepted April 15, 2026

DOI: 10.3892/ijmm.2026.5841

Abstract. Ferroptosis exerts a recognized role in the pathogenesis of acute kidney injury (AKI) and is considered a critical target for improving its prognosis. Emerging evidence indicates that ferroptosis serves a pivotal role in pathogenesis of AKI and targeting ferroptosis provides a promising therapeutic strategy in treatment of AKI. In the present study, ligustroflavone (LIG), which is a flavonoid with oral activity extracted from *Ligustrum lucidum*, was found to inhibit ferroptosis through activation of nuclear factor erythroid 2-related factor 2 (NRF2) via inhibition of GSK3β *in vivo* and *in vitro*. *In vivo*, cisplatin (CDDP) and ischemia-reperfusion injury (IRI)-induced murine models of AKI were constructed to evaluate the possible effects of LIG. *In vitro*, the protective effects of LIG were assessed in cultured mouse renal proximal tubular epithelial cells (TKPTs). Immunostaining, reverse transcription-quantitative PCR, western blot and lipid peroxidation assays were performed to detect renal tubular injury and ferroptosis. The results of the present study demonstrated that LIG administration significantly ameliorated CDDP or IRI induced renal damage in mice. Additionally, administration of LIG significantly ameliorated lipid peroxide accumulation and inhibited ferroptosis in the kidneys of AKI mice. *In vitro*, LIG treatment markedly ameliorated CDDP-induced lipid peroxidation and ferroptosis in cultured TKPTs via GSK3β inhibition and NRF2 activation. Furthermore, knockout of GSK3β also protected against CDDP-induced cell death and LIG exerted no additional protective effects in GSK3β-knockout TKPTs. Together, the present findings offer a new potential strategy for AKI therapies by targeting ferroptosis.

Correspondence to: Dr Yunwen Yang, Nanjing Key Laboratory of Pediatrics, Children's Hospital of Nanjing Medical University, 72 Guangzhou Road, Nanjing, Jiangsu 210008, P.R. China
E-mail: yangyunwen@njmu.edu.cn

Dr Fangfang Cai, Department of Cell Biology, School of Basic Medical Sciences, Nanjing Medical University, 101 Longmian Avenue, Jiangning, Nanjing, Jiangsu 211166, P.R. China
E-mail: caifangfang@njmu.edu.cn

*Contributed equally

Abbreviations: AKI, acute kidney injury; CDDP, cisplatin; IRI, ischemia/reperfusion injury; TKPTs, mouse renal proximal tubular epithelial cells; BUN, blood urea nitrogen; SCr, serum creatinine; NRF2, nuclear factor erythroid 2-related factor 2; GSK3β, glycogen synthase kinase 3β; LIG, ligustroflavone; PAS, periodic acid-Schiff; TUNEL, terminal deoxynucleotidyl-transferase-mediated dUTP nick end labeling; CETSA, cellular thermal shift assay

Key words: AKI, LIG, ferroptosis, GSK3β, NRF2

Introduction

Acute kidney injury (AKI) is marked by a rapid decline in renal function, together with concurrent structural and functional impairment of the kidneys (1). Clinical manifestations include the accumulation of nitrogenous metabolic products in the body including blood urea nitrogen (BUN) and serum creatinine (SCr) or oliguria (2). AKI is prevalent among hospitalized patients (with incidence rate more than 10%), particularly those who are critically ill, and is attributed to drugs, ischemia and renal obstruction. The exact pathogenesis remains a matter of debate (3). This underscores the need to explore novel treatment approaches.

Renal tubular epithelial cells (RTECs) are the primary cells damaged by AKI (4). Following injury, RTECs undergo pathological alterations such as degeneration, apoptosis, necrosis and shedding (5). Previous studies have indicated that both patients with AKI and AKI animal models display iron and lipid metabolism dysregulation, ultimately resulting in

ferroptosis in RTECs (6,7). Ferroptosis is an iron-dependent form of programmed cell death that manifests as mitochondrial structural damage and lipid peroxidation, with specific triggers, regulators and effectors (8). Nuclear factor erythroid 2-related factor 2 (NRF2) is an antioxidant transcription factor that directly or indirectly affects ferroptosis through various pathways. Previous studies have shown that the NRF2 pathway has the potential to alleviate iron cell death-related pathological damage and is a key target for disease intervention (9-11). Glycogen synthase kinase 3β (GSK3β), a key negative regulator of NRF2, triggers the ubiquitination and degradation of NRF2. Additionally, active GSK3β promotes the recognition and binding of NRF2 by β-transducin repeat-containing proteins (β-TrCPs) via phosphorylation of the Ser335 and Ser338 sites within the Neh6 domain of NRF2, consequently, promoting Kelch-like ECH-associated protein 1 (KEAP1)-mediated ubiquitination of NRF2 and the subsequent proteasome-dependent degradation of NRF2 (12). Previous studies have demonstrated that direct disruption of the NRF2-KEAP1 protein to protein interaction induces NRF2 activation and shows protective effects in AKI (13,14). Therefore, targeting the GSK3b-NRF2 signaling axis is another possible effective approach for NRF2 activation to inhibit ferroptosis and improve AKI.

The traditional Chinese medicine (TCM) *Ligustrum lucidum* has long been employed in renal tonification therapy for several decades, attributed to its remarkable efficacy and low incidence of adverse reactions (15). *Ligustrum lucidum* was first recorded in Shen Nong's Herbal Classic, is also found in the Compendium of Materia Medica, and is noted as a herb without obvious toxicity (16). Recent studies have identified ligustroflavone (LIG; also known as nuezhenoside), which is a flavonoid with oral activity extracted from *Ligustrum lucidum*. The chemical formula of LIG is $C_{33}H_{40}O_{18}$ with a molecular weight of 724.66 g/mol. To date, LIG has been reported to exert protective effects against ischemic stroke, diabetes-induced osteoporosis and liver fibrosis (17-19). LIG exhibits neuroprotective pharmacological effects by enhancing neurological function and reducing brain tissue damage in ischemic stroke models by targeting receptor-interacting serine/threonine-protein kinase 1/3 (RIPK1/3) and mixed lineage kinase domain like pseudokinase (MLKL) to inhibit necroptosis (17), while downregulating the NLR family pyrin domain containing 1 (NLRP1) inflammasome and cytokines (20). In anti-liver fibrosis, LIG downregulates TGF-β/Smad signaling, inhibits hepatic stellate cell activation and collagen deposition, reduces serum ALT/AST levels and alleviates liver tissue oxidative damage (18). For regulation of calcium metabolism and anti-osteoporosis LIG acts as a calcium-sensing receptor antagonist, promotes parathyroid hormone release to regulate calcium balance and improves bone mineral density and bone microstructure in diabetic model mice (19). LIG also exhibits anti-inflammatory effects which support the anti-inflammatory application of *Ligustrum* plants in traditional Mediterranean medicine (21).

However, there have been no relevant reports on the application value of LIG for the treatment of AKI. Therefore, the present research seeks to further evaluate the potential renoprotective effect of LIG on AKI and its underlying mechanism.

Materials and methods

LIG. LIG, with a purity of 99.90%, was procured from TargetMol Chemicals, Inc. (Targetmol; cat. no. T3802). As a naturally flavonoid, LIG was isolated from the common plant *Ligustrum lucidum*. In the present study, for animal experiments, LIG was fully dissolved in the solvent [10% dimethyl sulfoxide (DMSO) + 40% PEG300 + 5% Tween-80 + 45% saline, v/v] as specified in the instructions provided by the manufacturer.

Experimental animal manipulation and medication. The experimental male mice bred on the C57BL/6J genetic background, with an average age of 8 weeks, were procured from the Laboratory Animal Center of Nanjing Medical University. All animals (54 mice, weighing 20-25 g) were housed individually under standard and environmentally controlled cages (12/12-h light/dark cycle, 22˚C) with free access to water and a commercial rodent diet to ensure their health and well-being. The experimental procedures strictly conformed to Chinese national standard [Guidelines for the Ethical Review of Laboratory Animal Welfare (GB/T 35892-20181) (22)] and were approved by the Animal Ethics Committee of Nanjing Medical University (approval no. 2310025-2).

All mice were allowed to acclimatize for a week before the present study and then were assigned by simple randomization. The operators were unaware of the respective group condition. Cisplatin (CDDP) injection and ischemia-reperfusion injury (IRI) were selected as AKI models. In the CDDP-induced AKI model, all mice were weighed and then orally administered LIG (15 or 30 mg/kg/day) or an equivalent solvent continuously for 3 days prior to AKI model. LIG was fully dissolved in the solvent (10% DMSO + 40% PEG300 + 5% Tween-80 + 45% saline, v/v) and the final volume of DMSO administered to mice was 1 μl/g/d. Humane endpoints were strictly followed throughout the experiment. Mice were humanely euthanized if they exhibited severe lethargy, significant weight loss (>20% of baseline body weight), inability to eat or drink, severe dyspnea, or sustained neurological dysfunction. The experimental groups were: Vehicle, LIG, vehicle + CDDP, and LIG + CDDP (n=6). At 3 days after a single intraperitoneal injection of saline vehicle or 20 mg/kg CDDP (cat. no. 232120; MilliporeSigma). Blood samples (300 ml per mouse) were collected from the inferior vena cava under general anesthesia. Mice were anesthetized with 5% isoflurane for induction, followed by 2.5% isoflurane for maintenance using a multi-channel small animal anesthesia system (R550, RWD Life Science). Under deep anesthesia, mice were euthanized by exsanguination, and kidney tissues were subsequently harvested for further analysis. The IRI experiment was conducted as previously described (23). All mice were organized into four groups: Vehicle, LIG, vehicle + IRI and LIG + IRI groups (n=6). Similarly, the mice were treated daily with LIG by gavage (30 mg/kg/day) 3 day prior to IRI surgery. Mice were anesthetized with 2.5% isoflurane, subjected to renal IRI surgery, and euthanized 24 h postoperatively. In addition, conventional indexes of Scr and BUN were detected by a standard biochemical analyzer, and renal tissues were stored at -80˚C for further analyses.

Cell culture. The TKPT cell line (ATCC; cat. no. CRL-3361) was cultured in Dulbecco's Modified Eagle Medium (DMEM)/F-12 medium (cat. no. 319075CL; Gibco; Thermo Fisher Scientific, Inc.) containing 10% fetal bovine serum (FBS; cat. no. 26170035; Gibco; Thermo Fisher Scientific, Inc.;) and 1% penicillin-streptomycin (cat. no. C0224; Beyotime Institute of Biotechnology) at 37˚C under a 5% CO_2 humidified atmosphere. For drug use, TKPTs ($1x10^6$) were initially incubated with selected concentrations of LIG for 24 h and then stimulated with 5 μg/ml CDDP (cat. no. P4394; MilliporeSigma) for another 24 h. The control group was given the equal volume of 0.1% DMSO (cat. no. D2650; MilliporeSigma). Total cellular proteins or RNA were harvested for subsequent analysis.

GSK3β-knockout (GSK3β-KO) TKPTs constructed: The CRISPR/Cas9 plasmids targeting mouse GSK3β [the guide (g) RNA sequences are presented in Table SI] were constructed by using PX459 (cat. no. 62988; Addgene, Inc.). gRNAs were designed using Benchling's CRISPR Guide RNA Design Tool (https://benchling.com/). gRNA1 targeted exon 1 of GSK3b, affecting the N-terminal regulatory region, while gRNA2 targeted exon 5, affecting the C-terminal catalytic lobe. Then the plasmids were transfected into TKPTs using Lipofectamine 2000 (cat. no. 11,668,030; Thermo Fisher Scientific, Inc.), and the positive cells were selected using puromycin (2 μg/ml) for 3 days prior to clonal expansion. PX459 was used as a negative control. Western blotting (WB) was performed to confirm the successful knockout of GSK3β.

Renal histopathological examinations. The preserved kidney tissues from mice were cut into 4-μm sections using a microtome. After deparaffination (Paraffin sections were deparaffinized in xylene for 5-10 min, repeated twice) and rehydration (through a graded ethanol series 100, 95, 85, 75%, 5 min each, and rinsed in distilled water), all slides were subjected to routine staining with periodic acid-Schiff (PAS) staining (cat. no. C0142S; Beyotime Institute of Biotechnology) synchronously, following the manufacturer's instructions. Briefly, after deparaffinization, the paraffin sections were immersed in distilled water. PAS oxidizing agent was applied to the sections, and incubated at room temperature for 5 min. The sections were rinsed with distilled water twice, 1 min each time. The sections were covered with Schiff's reagent and stained in the dark for 10 min, before rinsing again with distilled water for 2 min. The nuclei were counterstained with hematoxylin for 2 min. The evaluation of renal pathological changes involved the assessing renal tubular dilation, brush border loss, tubular cell necrosis, intratubular cell detachment and cast formation. The pathological indicators of each manifestation were graded using a semi-quantitative scoring method: 0 (no damage), 1 (<25), 2 (25-50%), 3 (50-75%) and 4 (>75%), referring to our previous study (24). The sum of the tubular injury score was separately calculated in ≥5 randomly different fields per sample (magnification, x400) by a professional brightfield microscope (BX51; Olympus Corporation).

Reverse transcription-quantitative PCR (RT-qPCR). RNA was obtained from fresh renal tissues of the model mice using the TRIzol kit (cat. no. 9108; Takara bio, Inc.). The extracted RNA was adjusted to a concentration of 1 μg/μl and reversely transcribed into cDNA following the manufacturer's protocol. The cDNA was amplified on the QuantStudio™ 3 system using SYBR Green Master Mix (cat. no. q111-02/03; Vazyme Biotech Co., Ltd.). Cycling conditions were as follows: 95˚C for 10 min, followed by 40 repeats of 15 sec at 95˚C for denaturation and 1 min at 60˚C for annealing and extension. The primers (Table SI) were synthesized by a biotechnology company (Beijing Tsingke Biotech Co., Ltd.). The mRNA levels were normalized to β-actin which was used as the reference gene and quantified using the $2^{-\Delta\Delta Cq}$ method (25).

WB. Protein was isolated from homogenized renal biopsies (30 mg/mouse) and TKPT cells ($2x10^6$) using RIPA buffer (cat. no. P0013B; Beyotime Institute of Biotechnology); subsequently, protein samples (30 μg) were subjected to 10% SDS-PAGE (cat. no. P0012A; Beyotime Institute of Biotechnology) under the condition of constant voltage of 120 V and transferred onto PVDF membranes (cat. no. IPFL00010; Merck KGaA). After blocking in 5% skim milk, the membranes were incubated with the targeted antibodies (Table SII) overnight at 4˚C, washed with Tris-buffered saline containing 0.02% Tween (TBST) and incubated with HRP-conjugated secondary antibodies at RT for 1 h. Following SuperSignal™ West Pico Chemiluminescent Substrate Kit (cat. no. 34577; Thermo Fisher Scientific, Inc.), the proteins bands were finally visualized using a chemiluminescence system (ChemiDoc™ ECL; Bio-Rad Laboratories, Inc.) and measured using ImageJ software (version 1.51; National Institutes of Health). For fraction WB, nuclear and cytoplasmic protein were extracted using a Nuclear and Cytoplasmic Protein Extraction Kit (cat. no. P0027; Beyotime Institute of Biotechnology). Then the protein samples were analyzed by WB.

Cell viability, cell death and cell injury assays. TKPT cells were cultured in 96-well v-bottom plates at $2x10^4$ cells per well and allowed to attach overnight with the appropriate growth medium. After the indicated drug treatment duration, the medium was replaced with the Cell Counting Kit-8 (CCK-8) reagent (cat. no. KGA317; Nanjing KeyGen Biotech Co., Ltd.). TKPT cells were incubated with CCK-8 medium (10 μl CCK8 + 90 μl serum-free cell culture medium per well) at 37˚C for 2 h, and the absorbance was measured at 450 nm using a commercial microplate absorbance reader (BioTek Synergy H1; Agilent Technologies, Inc.). The percentage of viable cells in each group was calculated and compared as a percentage relative to untreated controls. Liproxstatin-1 was used as the ferroptosis inhibitor control because it is a highly potent, stable, and widely accepted canonical inhibitor. Compared with ferrostatin-1, liproxstatin-1 shows greater metabolic stability and comparable or higher inhibitory efficacy, making it more suitable for our experimental system. Extensive literature confirms liproxstatin-1 as a reliable positive control to verify ferroptosis (26), thus justifying its use as the sole inhibitor. For ferroptosis-specific rescue experiments, liproxstatin-1 (cat. no. HY-12726; MedChemExpress) was used as a ferroptosis-specific inhibitor in the present study.

In the cell death assay, a common BrightGreen kit (cat. no. A112-01/02/03; Vazyme Biotech Co., Ltd.) was utilized for TUNEL staining. Initially, 4-μm frozen renal tissue sections

were fixed with 4% paraformaldehyde at room temperature to preserve the integrity of the cellular structure. Subsequently, the slides were treated with 0.1% Triton X-100 at room temperature for 5 min. Then, the TdT enzyme recommended by the kit, along with fluorescently labeled dUTP, was added to the samples. After washing, the samples were dried in the dark, mounted with an anti-fade mounting medium and observed under a fluorescence microscope (Carl Zeiss AG). Finally, the positive green fluorescent cell counts were calculated.

In addition, TKPT cell injury was also analyzed. The cells were cultured in 12-well plates at $2x10^5$ cells per well and allowed to attach overnight with the appropriate growth medium. The cells were incubated with CDDP (5 mg/ml) with or without LIG treatment (20 μM) for 24 h. The cell supernatant was collected by centrifugation (5,000 x g) at 4˚C for 5 min. The lactate dehydrogenase (LDH) levels in the supernatant were detected using a LDH Release Assay Kit (cat. no. C0016; Beyotime Institute of Biotechnology) according to the manufacturer's instructions.

Cellular thermal shift assay (CETSA). In vitro, the target proteins of LIG were identified using the CETSA method (27). TKPTs were seeded on culture plates and treated with 20 μM LIG. The supernatant of the cell lysate was heated for 3 min in a Veriti thermal cycler (Applied Biosystems; Thermo Fisher Scientific, Inc.) at temperatures ranging from 42 to 52˚C, then cooled at 4˚C for 3 min. The heat-denatured precipitated proteins were removed by centrifugation. The target proteins were quantified via WB, and the melting curve of soluble GSK3β protein was plotted using GraphPad (version 6.01; Dotmatics).

Immunohistochemical (IHC) staining. Briefly, the mouse kidneys were fixed and cut into 4-μm sections. IHC staining was performed on all samples from each group, with three sections for each sample. Further steps of dewaxing, hydration, antigen retrieval, inactivation of endogenous enzymes and blocking were carried out following standard protocols (28). To characterize inflammatory levels of the affected kidney, immunostaining was performed on kidney sections using primary antibodies for F4/80 (1:100; cat. no. 70076; Cell Signaling Technology, Inc.) at 4˚C overnight and then incubated with SignalStain® Boost IHC Detection Reagent (HRP, Rabbit) (cat. no. 8114S; Cell Signaling Technology, Inc.) as the secondary antibody at room temperature for 1 h. A total of 5 microscopic images were captured randomly from each section (magnification, x40). Subsequently, representative images were imaged using a digital slide scanner (Olympus Corporation). Finally, the integrated optical density (IOD) values of each visual field were quantified using ImageJ software (1.51j8; National Institutes of Health), and a semi-quantitative analysis of F4/80 expression was analyzed.

Immunofluorescence (IF) staining and confocal microscopy. For IF staining, the renal sections (4 μm) were dewaxed, then antigen retrieval for the paraffin-embedded renal sections was performed using the microwave heating method in citrate antigen retrieval solution (cat. no. P0083; Beyotime Institute of Biotechnology). Selected sections were incubated with 10% FBS containing 0.3% Triton-X-100. The slides were immunostained using primary antibodies (Table SIII). Subsequently, secondary antibodies (listed in Table SIII) were applied and DAPI (cat. no. C1006; Beyotime Institute of Biotechnology) was employed to stain cell nuclei. All sections were then visualized with a confocal laser microscope (Carl Zeiss AG).

Transmission electron microscopy (TEM). The maximum size of 1 mm^3 fresh renal cortex tissue was fixed with 1.25% glutaraldehyde, post-fixation using 1% osmium tetroxide and embedded in a mold filled with epoxy resin in accordance with our previous study (13). The tissues were then sectioned into ultrathin slices measuring 60-90 nm in thickness and mounted on nickel grids. These sections were double-stained with uranyl acetate and lead citrate. The ultrastructure of mitochondria within renal tubules was examined using TEM (JEOL, Ltd.). Mitochondrial morphological alterations associated with ferroptosis were evaluated under TEM. Cells exhibiting mitochondrial shrinkage, increased matrix electron density, reduced or disorganized cristae, and outer mitochondrial membrane disruption were defined as ferroptosis-related damaged mitochondria. These morphological features were assessed in at least five randomly selected fields per sample, and representative images were acquired for quantitative and qualitative analysis.

Cellular iron assay. In the analysis system of renal iron metabolism, the levels of ferrous ion (Fe^{2+}) content both in the kidney tissues and cultured cells were measured by using a Ferrous Ion Content Assay Kit (cat. no. BC5410; Beijing Solarbio Science & Technology Co., Ltd.). Firstly, 0.1 g mouse kidney tissue was accurately weighed, 1 ml extraction buffer was added to homogenize these samples on ice and they were centrifuged (5,000 x g) at 4˚C for 5 min to collect the supernatant. Afterward, a standard curve was prepared with reference compounds according to the instructions of the manufacturer and the absorbance was measured at 593 nm using a common microplate reader (BioTek Synergy H1; Agilent Technologies, Inc.). Finally, the Fe^{2+} levels (mM/mg) were calculated based on the sample mass.

Lipid peroxidation assays. C11-BODIPY™ 581/591 (cat. no. D3861; Thermo Fisher Scientific, Inc.), a lipid-soluble ratio metric fluorescent indicator, was employed to detect cellular lipid peroxidation levels. As per the manufacturer's instructions, ~10^6 TKPT cells were seeded on round coverslips overnight. Subsequently, the TKPTs were stained by 5 μM BODIPY for 30 min at room temperature and washed with PBS. Upon oxidation, mean fluorescence intensity (MFI) was observed using a fluorescent microscope (LSM 900; Carl Zeiss AG) at an excitation wavelength shifting from 581 to 500 nm and an emission shifting from 591 to 510 nm. The levels of malondialdehyde (MDA) and the relative ratio of glutathione (GSH) to glutathione disulfide (GSSG) were utilized to detect membrane lipid peroxidation in renal tissues or TKPT cells. Briefly, the activity of MDA for the experimental samples was detected using a Lipid Peroxidation MDA Assay Kit (cat. no. S0131; Beyotime Institute of Biotechnology), while the GSH/GSSG ratio was evaluated with a GSH and GSSG Assay Kit (cat. no. S0053; Beyotime Institute of Biotechnology).

The absorbances were measured using a common microplate reader (BioTek Synergy H1; Agilent Technologies, Inc.).

LIG targets analysis and molecular docking. The potential targets of LIG were predicted using the Swisstarget prediction software (https://swisstargetprediction.ch/). The crystal structure of GSK3β employed for molecular docking was retrieved from the RCSB Protein Data Bank (PDB ID: 1H8F). The three-dimensional structure of LIG (PubChem Compound CID: 10417462) was obtained from the PubChem database as a candidate ligand targeting GSK3β. Molecular docking simulations between LIG and GSK3β were conducted using AutoDock Vina (version 4.2.6), an open-source tool developed by the Center for Computational Structural Biology at Scripps Research, to evaluate their potential binding interaction. All generated docking conformations were re-evaluated using the GBVI/WSA dG scoring function, with binding affinities expressed in kcal/mol. The binding conformation corresponding to the minimum binding free energy was defined as the optimal binding mode (29). The molecular interaction patterns derived from docking were further visualized and analyzed using PyMOL (v2.6.2; Schrödinger, Inc.), a molecular visualization system originally developed by Warren L. DeLano.

Statistical analyses. Statistical analyses were performed using GraphPad Prism 6.01 or IBM SPSS 13.0 (SPSS, Inc.) statistics software. All data presented in the figures are expressed as the mean ± SD. For animal models, a sample size of n=6 per group was chosen based on previous studies with similar experimental designs and models (30,31), as well as results from the authors' preliminary experiments. This sample size was considered adequate to ensure the reliability of statistical comparisons and to meet the ethical requirements for animal use, all cell experiments replicated three times or more. Normality of the data was tested using the Shapiro-Wilk test. Results confirmed that the data were normally distributed, so parametric tests were used for subsequent statistical analysis. Group differences were analyzed using one- or two-way analysis of variance (ANOVA) with Tukey's post hoc multiple comparisons test. $P<0.05$ was considered to indicate a statistically significant difference.

Results

LIG mitigates AKI induced by CDDP in a murine model. To investigate the potential therapeutic role of LIG in AKI, a well-characterized CDDP-induced AKI mouse model was established with LIG administered via intragastric gavage. A dose of 15 mg/kg LIG could enhance BUN level in AKI mouse, yet it had no significant impact on Scr. Following 20 mg/kg CDDP administration, Scr and BUN levels in mice were significantly elevated. Treatment with 30 mg/kg LIG significantly improved renal function, as evidenced by reduced SCr and BUN levels (Fig. 1A). Furthermore, histopathological evaluation revealed that LIG treatment significantly ameliorated tubular injury in the CDDP-induced AKI model (Fig. 1B). PAS staining was employed to assess renal morphological changes. In CDDP-treated mice, marked tubular necrosis, dilation and protein cast formation were observed (Fig. 1C). However, LIG treatment effectively mitigated these pathological alterations. To further validate the protective effects of LIG, WB was performed to evaluate kidney injury molecule-1 (KIM-1) and neutrophil gelatinase-associated lipocalin (NGAL). The results demonstrated that KIM-1 and NGAL expression levels were markedly elevated in the kidneys of AKI mice compared with the control group, whereas LIG treatment significantly downregulated their expression (Fig. 1D). Notably, LIG alone did not affect renal function or morphology. These findings indicate that LIG exerts a protective effect against CDDP-induced AKI.

LIG reduces tubular apoptosis and inflammatory response. To assess CDDP-induced apoptosis, TUNEL staining was performed. The results revealed a significant increase in TUNEL-positive cells in the CDDP group, which was significantly reduced following LIG treatment, approaching the levels observed in the normal control group. No significant changes in cell apoptosis were observed in healthy mice treated with LIG alone (Fig. 2A). To elucidate the underlying anti-apoptotic mechanism, WB was employed to evaluate the expression of cleaved caspase 3, a key executor of apoptosis. LIG significantly attenuated the CDDP-induced increase in cleaved caspase 3 expression, thereby reducing apoptosis (Fig. 2B). Moreover, protein expression of phosphorylated RIP3 (Ser232), a hallmark of necroptosis, was not reduced by LIG, suggesting that LIG does not alleviate CDDP-triggered necroptosis (Fig. 2B). Histological analysis further demonstrated that LIG administration significantly decreased the number of F4/80-positive cells in the kidneys of CDDP-treated mice (Fig. 2C). Furthermore, RT-qPCR analysis was performed to assess the mRNA expression of proinflammatory genes, including TNFα, IL-1β, IL6 and MCP1, in mouse kidneys. The results revealed that CDDP-induced upregulation of TNFα, IL-1β, IL6 and MCP1 mRNA levels was significantly attenuated by LIG treatment (Fig. 2D). These results suggest that LIG suppresses macrophage infiltration and the associated inflammatory response in the kidney.

LIG activates NRF2 by inhibiting GSK3β in vivo and in vitro. To further elucidate the molecular mechanisms of LIG against CDDP-induced AKI, the potential targets of LIG were predicted using the Swisstarget prediction software. Additionally, molecular docking of these potential targets was performed using AutoDock (version 4.2.6) to determine the molecules interacting with LIG. Among these possible targets, LIG exhibited the highest binding affinity with GSK3β (Fig. 3A). A three-dimensional molecular interaction model was constructed to investigate the spatial interaction between LIG and GSK3β (Fig. 3B), suggesting a possible direct binding at the molecular level.

The cytotoxicity of LIG was assessed using a CCK-8 assay, which demonstrated that concentrations <200 μM did not significantly affect cell viability (Fig. S1A). Additionally, CETSA results indicated that LIG enhanced the thermal stability of GSK3β, indicating that LIG may bind directly to GSK3β (Fig. 3C). Previous studies have reported that phosphorylation of GSK3b at serine 9 (Ser9) and tyrosine 216 (Tyr216) reflects its inhibition and activation, respectively (32,33). In the present study, the phosphorylation level

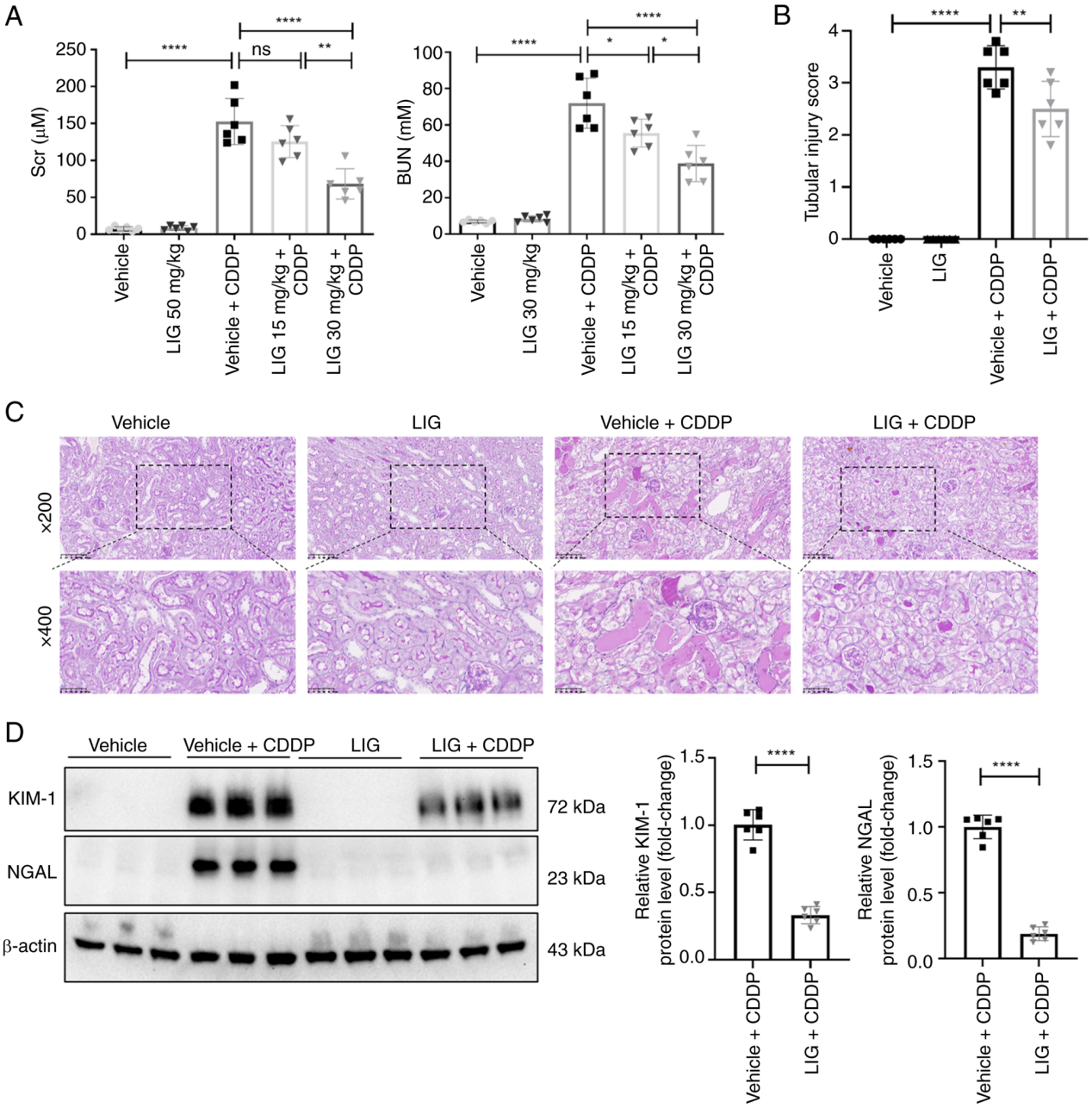

Figure 1. LIG mitigates acute kidney injury induced by CDDP in a murine model. (A) SCr and BUN levels in mice. (B) Calculation of tubular injury score based on PAS staining. (C) PAS staining for renal histopathology (magnification, x200 and x400). (D) Western blotting detection of the expression of tubular injury molecules KIM-1 and NGAL and semi-quantitative analysis of protein band intensities is presented on the right (n=6). *P<0.05, **P<0.01 and ****P<0.0001, (one-way ANOVA or unpaired t-test). LIG, ligustroflavone; CDDP, cisplatin; SCr, serum creatinine; BUN, blood urea nitrogen; PAS, periodic acid-Schiff; KIM-1, kidney injury molecule-1; NGAL, neutrophil gelatinase-associated lipocalin; vehicle, control; ns, not significant.

of GSK3b at Ser9 was examined to determine whether LIG could suppress the activity of GSK3b. For these reasons, the phosphorylation level of GSK3β at Ser9 was only analyzed. WB and semi-quantitative analysis revealed that LIG promoted the phosphorylation of GSK3β at Ser9 in a concentration-dependent manner (Figs. 3D and S1B). NRF2, a pivotal antioxidant transcription factor (25), exhibited enhanced expression and nuclear translocation in response to LIG treatment (Figs. 3E and S1C). The expression of glutathione peroxidase 4 (GPX4), heme oxygenase-1 (HO-1), NADPH quinone oxidoreductase 1 and solute carrier family 7 member 11, well-characterized transcriptional targets of NRF2 in TKPTs were next examined following LIG treatment. The data demonstrated that LIG dose-dependently increased both mRNA and protein levels of these target genes (Figs. 3F and S1D and E). Additionally, whether LIG treatment activates NRF2 in mouse kidneys was assessed. Mice were administered LIG (30 mg/kg/day) or vehicle by oral gavage for 72 h. WB (Figs. 3G and S1F) and IF staining (Fig. 3H) revealed that treatment with 30 mg/kg/day LIG markedly activated NRF2 via inhibition of GSK3β in mouse kidneys. Collectively, these findings demonstrate that LIG mitigates AKI, potentially through activation of the GSK3β/NRF2 pathway.

LIG protects against AKI by inhibiting ferroptosis in mice. In the present experiments, CDDP-induced AKI was associated

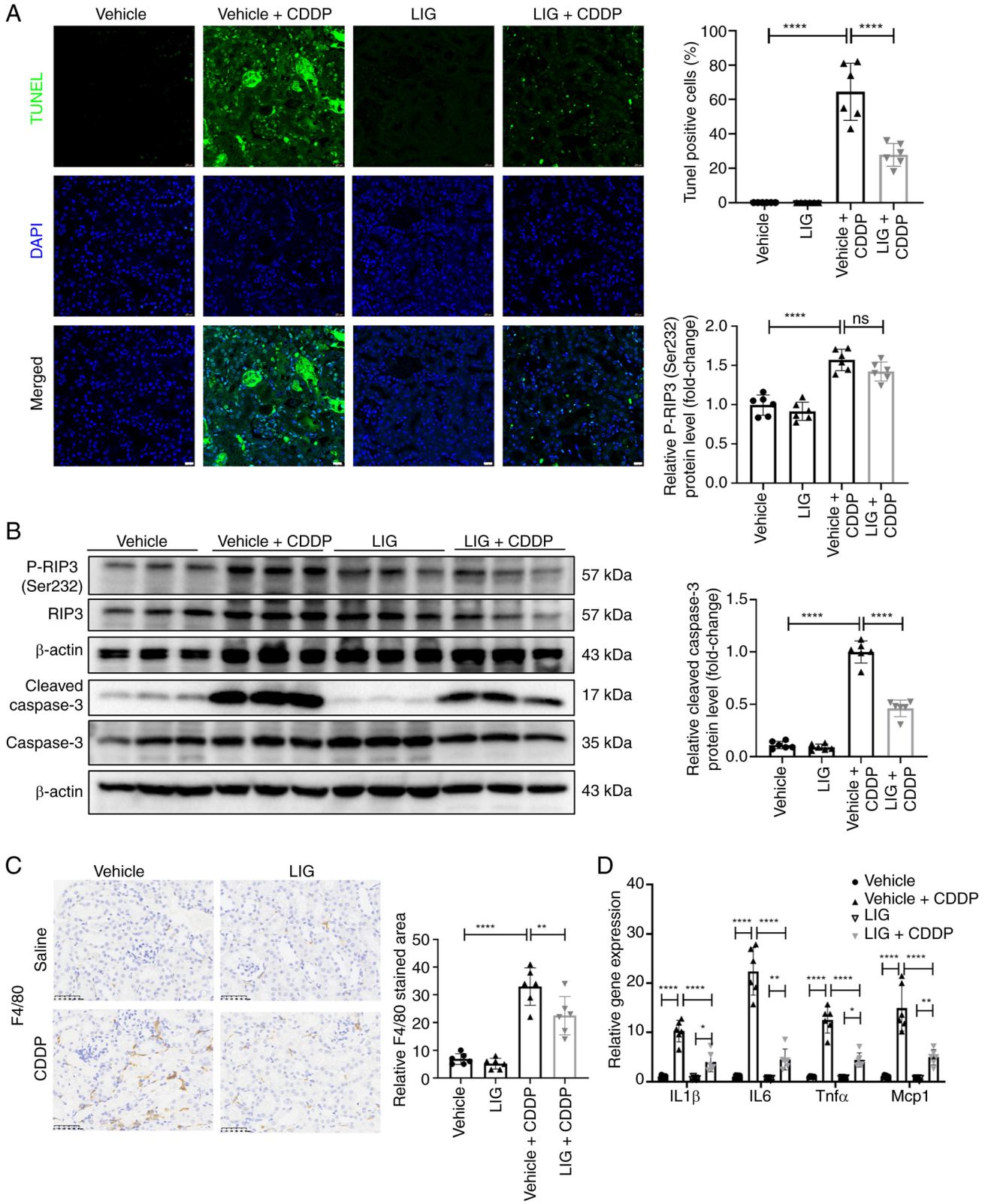

Figure 2. LIG treatment reduces cell apoptosis and inflammatory response in acute kidney injury. (A) TUNEL staining and quantitative analysis were conducted, with corresponding images generated. (B) The expression of cleaved caspase-3 was assessed using western blotting. (C) The staining distribution of F4/80 was evaluated using immunohistochemistry. (D) The mRNA levels of inflammatory genes including TNF, IL1β, IL-6 and MCP1 in kidneys of cisplatin-induced mice with or without LIG (30 mg/kg/day) treatment were analyzed using reverse transcription-quantitative PCR. The results are expressed as the mean ± SD of 6 mice in each group. *P<0.05, **P<0.01 and ****P<0.0001 (one-way ANOVA or unpaired t-test). LIG, ligustroflavone; CDDP, cisplatin; P-, phosphorylated.

with increased Fe^{2+} concentration (Fig. 4A), elevated MDA levels (Fig. 4B), reduced GSH/GSSG ratio (Fig. 4C) and dysregulated expression of metabolic genes (Fig. 4D). All these abnormal levels were markedly improved by LIG treatment, indicating the involvement of anti-ferroptosis effects of LIG in protecting against AKI. Additionally, WB analysis

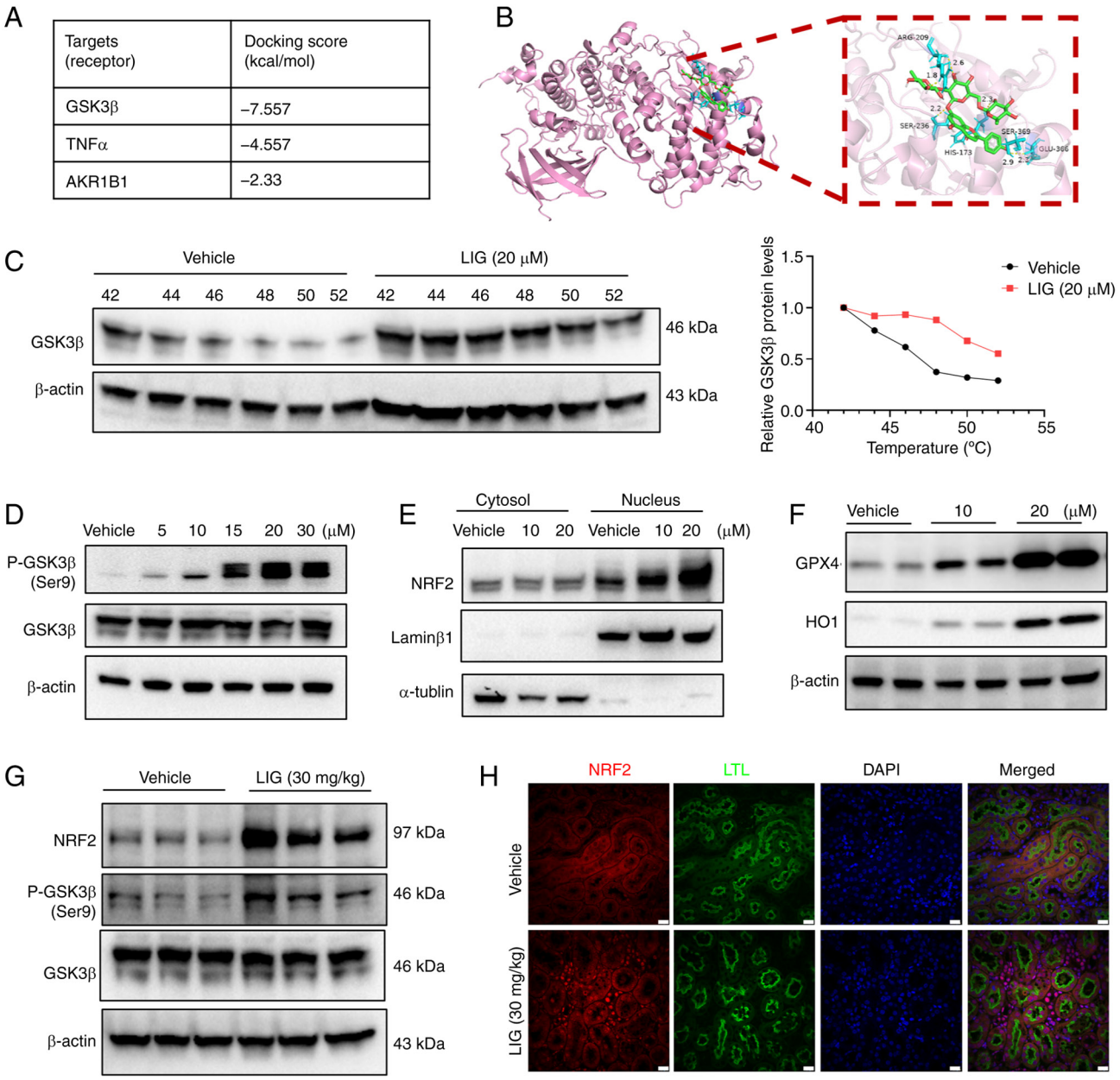

Figure 3. LIG activates NRF2 by inhibiting GSK3β to improve acute kidney injury. (A) Molecular docking analysis of the candidate targets with LIG. (B) A three-dimensional molecular interaction model. (C) A cellular thermal shift assay was performed to verify the direct binding of LIG to GSK3β. (D) WB of GSK3β and its phosphorylation in TKPTs treatment with LIG (0, 5, 10, 15, 20, 30 μM) for 24 h, the semi-quantitative analysis of protein band intensities is presented on Fig. S1B. (E) Subcellular localization of NRF2 were analyzed by fraction western blot in TKPTs treated with LIG (10, 20 μM) for 24 h, the semi-quantitative analysis of protein band intensities is presented on Fig. S1C. (F) WB of GPX4 and HO-1 in TKPTs treatment with LIG (10, 20 μM) for 24 h, the semi-quantitative analysis of protein band intensities is presented on Fig. S1D. (G) The protein levels of NRF2 and p-GSK3β (Ser9) in mice kidneys daily gavage with LIG (30 mg/kg/day) or vehicle for 72 h, the semi-quantitative analysis of protein band intensities is presented on Fig. S1F. (H) Immunofluorescent staining of NRF2, LTL and DAPI in mice kidneys daily gavage with LIG (30 mg/kg/day) or vehicle for 72 h. LIG, ligustroflavone; NRF2, nuclear factor erythroid 2-related factor 2; GSK3β, glycogen synthase kinase 3β; TKPTs, mouse renal proximal tubular epithelial cells; WB, western blotting; p-, phosphorylated; LTL, *Lotus tetragonolobus* lectin.

revealed that LIG treatment upregulated GPX4 expression, downregulated MPO expression and inhibited GSK3β activity (Fig. 4E), indicating suppression of ferroptosis by LIG treatment. At the mitochondrial level, LIG enhanced the expression of ATP synthase subunit b (ATPB) and superoxide dismutase 2 (SOD2), thereby improving mitochondrial antioxidant capacity (Fig. 4F). IF staining further demonstrated a significant decrease in the lipid peroxidation marker 4-hydroxynonenal (4-HNE) following LIG treatment (Fig. 4G). TEM showed that LIG reduced ferroptosis-related mitochondrial damage induced by CDDP (Fig. 4H). These findings suggest that LIG protects against AKI by inhibiting ferroptosis.

LIG alleviates CDDP-induced cellular oxidative damage and exerts a protective effect dependent on GSK3β. In vivo studies demonstrated that LIG mitigates CDDP-induced AKI by modulating oxidative stress, lipid peroxidation and the GSK3/NRF2 signaling pathway. To validate these findings *in vitro*, a CDDP-induced cell injury model was established. Exposure to CDDP significantly reduced cell viability (Fig. 5A), increased

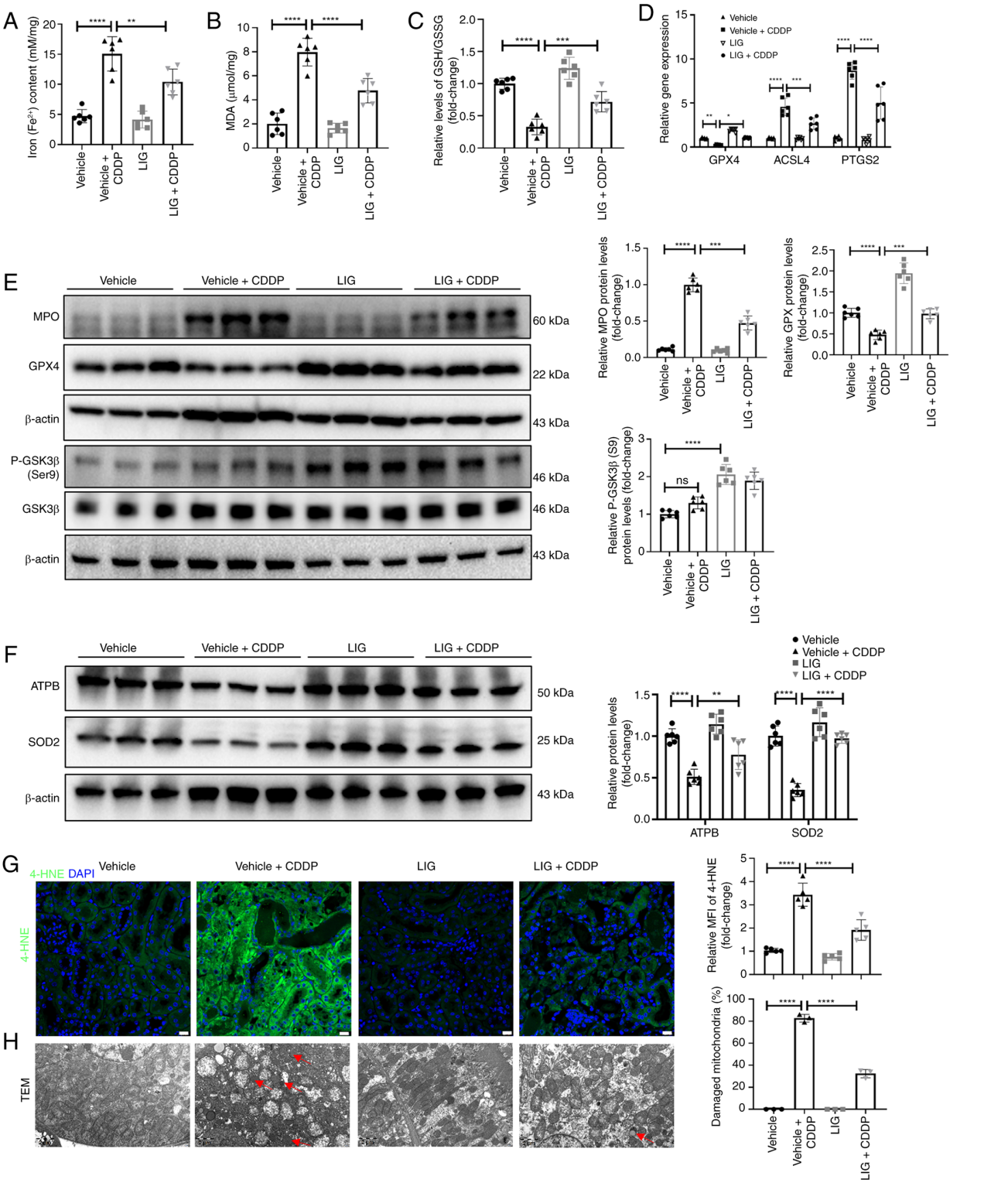

Figure 4. LIG treats acute kidney injury by inhibiting the ferroptosis pathway. (A) The concentration of Fe^{2+} levels. (B) The levels of MDA. (C) The GSH/GSSG ratio. (D) The expression of genes related to ferroptosis. (E) WB analysis the protein levels of GPX4, MPO and p-GSK3β (Ser9) in mice kidneys daily gavage with LIG (30 mg/kg/day) or vehicle then treated with cisplatin (20 mg/kg) for 72 h. (F) WB analysis the protein levels of ATPB and SOD2 in mice kidneys. (G) Immunofluorescent staining for 4-HNE in mice kidneys. (H) Transmission electron microscopy observation of mitochondrial damage in mice kidneys, the ferroptosis-related damaged mitochondria characterized by mitochondrial atrophy, reduced or even disappearing cristae and increased membrane density is indicated by red arrow. *P<0.05, **P<0.01, ***P<0.001 and ****P<0.0001 (one-way ANOVA or two-way ANOVA). LIG, ligustroflavone; MDA, malondialdehyde; GSH, reduced glutathione; GSSG, glutathione disulfide; WB, western blotting; GPX4, glutathione peroxidase 4; MPO, myeloperoxidase; p-, phosphorylated; GSK3β, glycogen synthase kinase 3β; ATPB, ATP synthase subunit b; SOD2, superoxide dismutase 2; 4-HNE, 4-hydroxynonenal; CDDP, cisplatin.

LDH release (Fig. 5B), elevated MDA levels (Fig. 5C) and decreased the GSH/GSSG ratio (Fig. 5D), indicating substantial oxidative stress and cellular damage. Enhanced BODIPY fluorescence further confirmed increased lipid peroxidation (Fig. 5E). However, LIG treatment effectively reversed these detrimental effects. Additionally, GSK3β-KO, was successfully

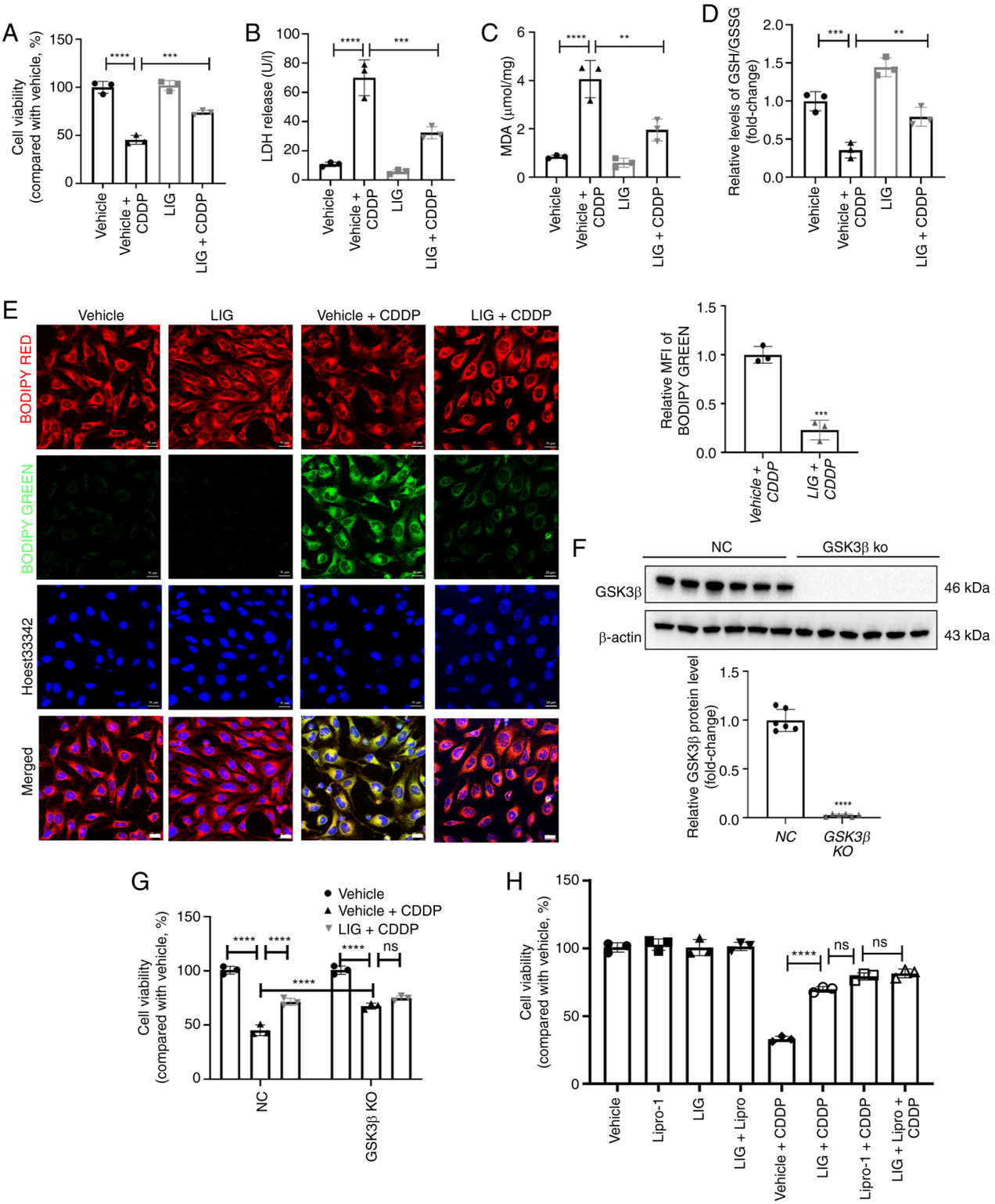

Figure 5. LIG protects against CDDP-induced damaged cells by regulating oxidative stress, lipid peroxidation and the GSK3β pathway. (A) Cell viability performed by CCK-8 assay in TKPTs treated with LIG (20 μM) and cisplatin (5 μg/ml) for 24 h. (B) LDH release was analyzed. (C) MDA levels were detected. (D) The GSH/GSSG ratio of TKPTs was analyzed. (E) Cisplatin induced lipid peroxidation in TKPTs were analyzed by staining with a BODIPY 581/591 C11 probe (green, oxidized lipids; blue, Hoechst; scale bar, 10 μm). (F) The successful construction of GSK3β-knockout TKPTs was analyzed using western blotting. (G) GSK3β-knockout and control TKPTs were treated with cisplatin with or without LIG treatment, and the cell viability was detected using CCK-8 assay. (H) TKPTs were treated with or without cisplatin for 24 h with lipro-1 (1 μM), LIG (20 μM) or LIG (20 μM) + lipro-1 (1 μM) treatment, and the cell viability was detected using a CCK-8 assay. The data are presented as the mean ± SD. **P<0.01, ***P<0.001 and ****P<0.0001 (one-way ANOVA or two-way ANOVA). LIG, ligustroflavone; CDDP, cisplatin; GSK3β, glycogen synthase kinase 3β; CCK-8, Cell Counting Kit-8; TKPTs, mouse renal proximal tubular epithelial cells; LDH, lactate dehydrogenase; MDA, malondialdehyde; GSH, reduced glutathione; GSSG, glutathione disulfide; lipro-1, liproxstatin-1; ns, not significant; NC, negative control.

established (Fig. 5F). The results showed GSK3β-KO significantly protected against CDDP-induced cell death. However, no additional protective effect of LIG was observed in GSK3β-KO TKPTs, as evidenced by cell viability measurements (Fig. 5G),

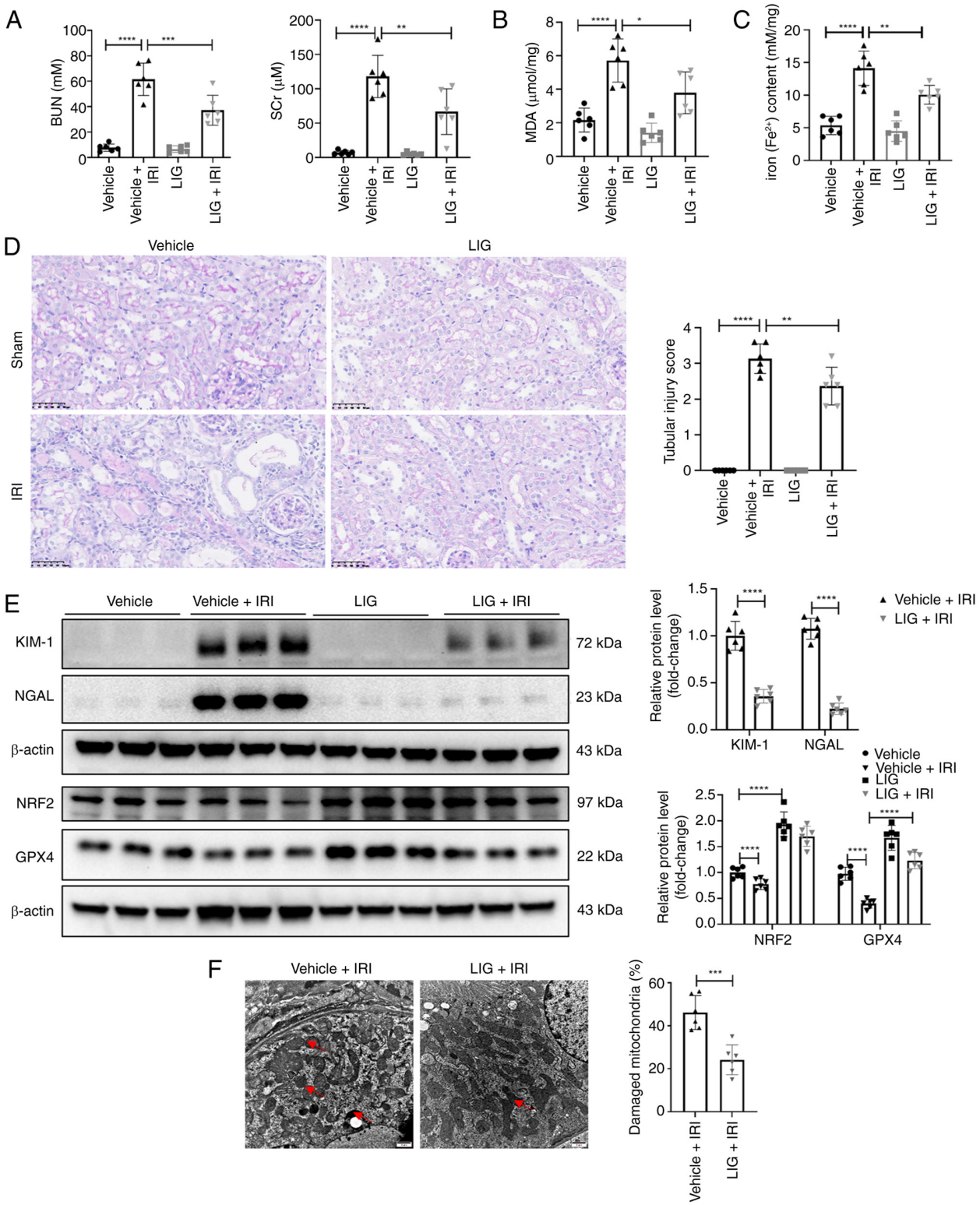

Figure 6. LIG prevents IRI-induced AKI by inhibiting ferroptosis. (A) BUN and SCr levels in IRI-induced AKI mice. (B) MDA levels in kidneys of mice with IRI-induced mice. (C) The concentration of Fe^{2+}. (D) Periodic acid-Schiff staining for renal histopathology. (E) Western blot analysis of KIM-1, NGAL, NRF2 and GPX4 expression. (F) Transmission electron microscopy observation of mitochondrial damage. *P<0.05, **P<0.01, ***P<0.001 and ****P<0.0001 (one-way ANOVA or two-way ANOVA). LIG, ligustroflavone; IRI, ischemia/reperfusion injury; AKI, acute kidney injury; BUN, blood urea nitrogen; SCr, serum creatinine; MDA, malondialdehyde; KIM-1, kidney injury molecule-1; NGAL, neutrophil gelatinase-associated lipocalin; NRF2, nuclear factor erythroid 2-related factor 2; GPX4, glutathione peroxidase 4.

suggesting that GSK3β serves a critical role in mediating the protective effects of LIG. The results also showed that LIG protected against CDDP-induced cell death similar to that of liproxstatin-1, a well-known ferroptosis inhibitor in TKPTS (Fig. 5H). Additionally, LIG exerted no additional protective effects in liproxstatin-1-treated TKPTs, suggesting that LIG protects against CDDP-induced cell death, at least in part by inhibiting ferroptosis. Overall, these *in vitro* results support the

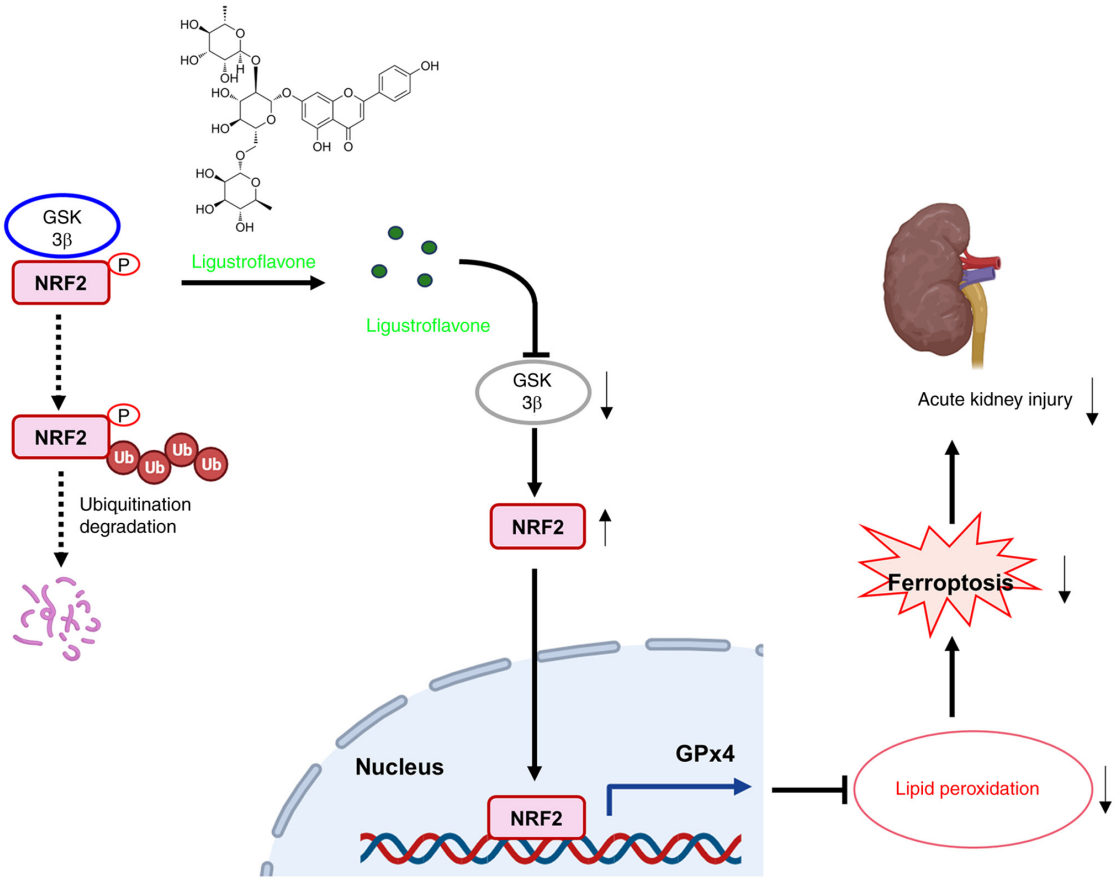

Figure 7. Schematic diagram of the present study. Overview of the role and mechanism of ligustroflavone in acute kidney injury. GSK3β, glycogen synthase kinase 3β; GPX4, glutathione peroxidase 4; NRF2, nuclear factor erythroid 2-related factor 2.

hypothesis that LIG protects against CDDP-induced oxidative stress and lipid peroxidation by affecting GSK3β signaling.

LIG prevents IRI-induced AKI by inhibiting ferroptosis. To further evaluate the therapeutic potential of LIG in different models of AKI, an IRI-induced AKI model was established, and LIG was administered via intragastric gavage. Similar to the CDDP model, IRI significantly increased SCr and BUN levels, which were markedly reduced following LIG treatment (Fig. 6A). Biochemical analysis revealed that LIG significantly attenuated the IRI-induced elevation of MDA levels (Fig. 6B) and Fe^{2+} content (Fig. 6C) in mouse kidneys, indicating suppression of lipid peroxidation. PAS staining confirmed that LIG attenuated tubular damage (Fig. 6D). TEM further demonstrated reduced mitochondrial injury. Moreover, LIG upregulated the expression of ferroptosis-inhibiting genes including NRF2 and GPX4, while downregulating kidney injury markers including KIM-1 and NGAL (Fig. 6E). TEM demonstrated that LIG reduced ferroptosis-related mitochondrial damage induced by IRI (Fig. 6F). These findings suggest that LIG protects against IRI-induced AKI by inhibiting ferroptosis.

Discussion

AKI is a prevalent clinical syndrome that carries a substantial burden of morbidity and elevated mortality (34). AKI can result in renal fibrosis and irreversible chronic kidney disease (CKD) (35). The etiology of AKI is multifactorial, with acute tubular necrosis, IRI and nephrotoxic agents being the primary causes (36). Recent research has indicated that both patients with AKI and AKI animal models exhibit disruptions in iron and lipid metabolism, culminating in iron-mediated cell death in RTECs (37,38). Therefore, targeting iron-mediated RTEC death holds promise as a therapeutic approach for AKI.

The present research demonstrated that LIG significantly shields renal tubular cells from CDDP-induced AKI by mitigating iron-mediated cell death. To elucidate the mechanism underlying the effects of LIG on AKI, IF, WB and lipid peroxidation assays were performed to assess alterations in the expression of MDA, GPX4 and other relevant indicators. The comprehensive experimental findings revealed that LIG confers renal protection primarily through the GSK3β/NRF2 pathway, thereby enhancing antioxidant defense mechanisms and mitigating cellular injury. In the group treated with CDDP, LIG markedly decreased renal injury markers, reflecting the protective effects of LIG. Furthermore, TUNEL staining and assessment of cleaved caspase-3 levels indicated that LIG suppressed apoptosis and mitigated the renal inflammatory response. The reduction in MPO activity and F4/80 expression further supported the notion that the inflammatory response was inhibited. Previous research has highlighted the antioxidant, anti-aging and anti-inflammatory properties of LIG (39), which align with its traditional use in Chinese medicine for conditions such as intestinal ischemia in perfusion injury (40), mental disorders (41) and diabetes (42). These findings are in line with the outcomes of the current study. Additionally, a previous study demonstrated that LIG was safe

and exhibited favorable bioavailability following oral administration, with rapid intestinal absorption and extensive *in vivo* metabolism in mice (19).

The present study revealed that LIG, a possible inhibitor of GSK3β, increased NRF2 nuclear translocation, which culminated in the activation of the cytoprotective NRF2 pathway (32,43). This NRF2 activation further triggers a suite of antioxidant genes, including GPX4, SOD2 and ATPB, with GPX4 being especially critical for the modulation of ferroptosis (44). The increase in GPX4 expression levels, the reduction in 4-HNE levels and the mitigation of lipid peroxidation strongly support the efficacy of LIG in ameliorating ferroptotic injury. According to previous studies, the GSK3β/NRF2 ferroptosis pathway serves a protective role in regulating ferroptosis in neurodegenerative diseases (45,46), ischemic cardiovascular and cerebrovascular diseases (47), liver injury (48) and other inflammation-related diseases (49,50).

GSK3β is widely expressed in the kidneys and has been demonstrated to be a positive regulator of ferroptosis. Knockdown of GSK3β decreases iron metabolism and the occurrence of ferroptosis (51). In LPS-induced AKI, a GSK3β inhibitor can promote the phosphorylation of GSK3β in renal tubules and facilitate the nuclear translocation of NRF2, leading to the upregulation of its downstream genes, such as HO-1 and NAD(P)H quinone oxidoreductase-1, thereby contributing to the amelioration of renal injury and the restoration of kidney function (52). Treatment with the novel GSK3β inhibitor 5n markedly alleviated renal damage and inflammatory expression in a CDDP-induced AKI mouse model, by interacting with PP2Ac to regulate the downstream activity of NF-κB (53). Furthermore, in a mouse model of kidney injury induced by folic acid, by targeting GSK3β in renal tubular cells, the NRF2 antioxidant response can be restored and the transformation of AKI to CKD can be prevented (54). In conclusion, the use of a new GSK3β inhibitor for preventing AKI may provide a potential strategy for the clinical treatment of AKI.

The present study is a novel investigation into the curative effect of LIG for the treatment of AKI. LIG could prevent iron-induced cell death via the GSK3β-NRF2 pathway, suggesting that it has promising therapeutic applications in AKI. However, some constraints still exist. The present study did not include ferroptosis-specific rescue experiments in animal models. Although NRF2 has numerous downstream targets, only the expression levels of HO-1 and GPX4 were analyzed. In addition, only one cell line was used in the present study. Finally, CDDP or IRI-induced AKI mice models can only partially reproduce AKI pathological damage in human. In summary, clinical drug trials for LIG need to be performed and its effectiveness further verified.

In conclusion, the present findings suggest that LIG effectively protects against AKI by mitigating oxidative stress and inflammatory response potentially via inhibiting ferroptosis (Fig. 7). These results not only enhance the comprehension of flavonoid-mediated renal defense but also provide a theoretical basis for the advancement of therapeutic approaches for AKI utilizing LIG.

Acknowledgements

Not applicable.

Funding

The present study was supported by the National Natural Science Foundation of China (grant nos. 82370683 and 82400816), the Natural Science Foundation of Jiangsu (grant no. BK20241731), the Nanjing Health Science and Technology Development Foundation (grant no. ZKX22049), the Nanjing Medical University Undergraduate Innovation Training Program Project (grant no. X2025103120062), the Youth Science and Technology Talent Support Program of Jiangsu (grant no. JSTJ-2025-121) and the Open subject of Jiangsu Key Laboratory of Brain Disease and Bioinformation (grant no. XZSYSKF2022025).

Availability of data and materials

The data generated in the present study may be requested from the corresponding author.

Authors' contributions

JSo wrote the original draft of the manuscript, developed methodology, conducted investigation and project administration, performed formal analysis and data curation, and provided resources. LW curated data, conducted project administration, formal analysis and investigation. YW developed methodology, conducted investigation, formal analysis and data curation, and conceptualized the study. JM and YZ developed methodology and conducted investigation. JSh wrote, reviewed and edited the manuscript, and conceptualized the study. SYX developed methodology. JL conducted formal analysis and data curation. FC wrote, reviewed and edited the manuscript, supervised the study, provided resources, conducted project administration and investigation, developed methodology, acquired funding, and performed formal analysis and data curation. YY wrote the original draft, wrote, reviewed and edited the manuscript, developed methodology, conducted investigation, formal analysis and project administration, curated data curation and acquired funding. JS and YY confirm the authenticity of all the raw data. All authors read and approved the final version of the manuscript.

Ethics approval and consent to participate

The present study was approved by the Animal Ethics Committee of Nanjing Medical University (approval no. 2310025-2; Nanjing, China).

Patient consent for publication

Not applicable.

Competing interests

The authors declare that they have no competing interests.

References

1. Ostermann M, Lumlertgul N, Jeong R, See E, Joannidis M and James M: Acute kidney injury. Lancet 405: 241-256, 2025.
2. Levey AS and James MT: Acute kidney injury. Ann Intern Med 167: ITC66-ITC80, 2017.

3. Bellomo R, Kellum JA and Ronco C: Acute kidney injury. Lancet 380: 756-766, 2012.
4. Gao J, Deng Q, Yu J, Wang C and Wei W: Role of renal tubular epithelial cells and macrophages in cisplatin-induced acute renal injury. Life Sci 339: 122450, 2024.
5. Li ZL, Li XY, Zhou Y, Wang B, Lv LL and Liu BC: Renal tubular epithelial cells response to injury in acute kidney injury. EBioMedicine 107: 105294, 2024.
6. Martin-Sanchez D, Ruiz-Andres O, Poveda J, Carrasco S, Cannata-Ortiz P, Sanchez-Niño MD, Ruiz Ortega M, Egido J, Linkermann A, Ortiz A and Sanz AB: Ferroptosis, but not necroptosis, is important in nephrotoxic folic acid-induced AKI. J Am Soc Nephrol 28: 218-229, 2017.
7. Guo R, Duan J, Pan S, Cheng F, Qiao Y, Feng Q, Liu D and Liu Z: The road from AKI to CKD: Molecular mechanisms and therapeutic targets of ferroptosis. Cell Death Dis 14: 426, 2023.
8. Zhao Z, Wu J, Xu H, Zhou C, Han B, Zhu H, Hu Z, Ma Z, Ming Z, Yao Y, *et al*: XJB-5-131 inhibited ferroptosis in tubular epithelial cells after ischemia-reperfusion injury. Cell Death Dis 11: 629, 2020.
9. Dodson M, Castro-Portuguez R and Zhang DD: NRF2 plays a critical role in mitigating lipid peroxidation and ferroptosis. Redox Biol 23: 101107, 2019.
10. He L, Chen Q, Wang L, Pu Y, Huang J, Cheng CK, Luo JY, Kang L, Lin X, Xiang L, *et al*: Activation of Nrf2 inhibits atherosclerosis in ApoE$^{-/-}$ mice through suppressing endothelial cell inflammation and lipid peroxidation. Redox Biol 74: 103229, 2024.
11. Ma F, Luo S, Lu C, Jiang X, Chen K, Deng J, Ma S and Li Z: The role of Nrf2 in periodontal disease by regulating lipid peroxidation, inflammation and apoptosis. Front Endocrinol (Lausanne) 13: 963451, 2022.
12. Li Y, Huang J, Wang J, Xia S, Ran H, Gao L, Feng C, Gui L, Zhou Z and Yuan J: Human umbilical cord-derived mesenchymal stem cell transplantation supplemented with curcumin improves the outcomes of ischemic stroke via AKT/GSK-3β/β-TrCP/Nrf2 axis. J Neuroinflammation 20: 49, 2023.
13. Cai F, Li D, Zhou K, Zhang W and Yang Y: Tiliroside attenuates acute kidney injury by inhibiting ferroptosis through the disruption of NRF2-KEAP1 interaction. Phytomedicine 126: 155407, 2024.
14. Shi Z, Zhang Y, Wang X, Tang J, Kang Y, Hu J, Li L, Yang B, Chen S, Xiao Q, *et al*: Discovery of propionic acid derivatives with a 5-THIQ core as potent and orally bioavailable keap1-Nrf2 protein-protein interaction inhibitors for acute kidney injury. J Med Chem 67: 19247-19266, 2024.
15. Zhang JL, Du C, Poon CCW, He MC, Wong MS, Wang NN and Zhang Y: Structural characterization and protective effect against renal fibrosis of polysaccharide from *Ligustrum lucidum* Ait. J Ethnopharmacol 302: 115898, 2023.
16. Wang YS, Jin YX, Liu KJ, Guo C, Wang YH, Xu C, Zhang ZX and Dong WP: Species identification of *Ligustrum lucidum*. Zhongguo Zhong Yao Za Zhi 48: 2940-2948, 2023 (In Chinese).
17. Zhang YY, Liu WN, Li YQ, Zhang XJ, Yang J, Luo XJ and Peng J: Ligustroflavone reduces necroptosis in rat brain after ischemic stroke through targeting RIPK1/RIPK3/MLKL pathway. Naunyn Schmiedebergs Arch Pharmacol 392: 1085-1095, 2019.
18. Kang R, Tian W, Cao W, Sun Y, Zhang HN, Feng YD, Li C, Li ZZ and Li XQ: Ligustroflavone ameliorates CCl_4-induced liver fibrosis through down-regulating the TGF-β/Smad signaling pathway. Chin J Nat Med 19: 170-180, 2021.
19. Feng R, Ding F, Mi XH, Liu SF, Jiang AL, Liu BH, Lian Y, Shi Q, Wang YJ and Zhang Y: Protective effects of ligustroflavone, an active compound from *Ligustrum* lucidum, on diabetes-induced osteoporosis in mice: A potential candidate as calcium-sensing receptor antagonist. Am J Chin Med 47: 457-476, 2019.
20. Bi F, Bai Y, Zhang Y and Liu W: Ligustroflavone exerts neuroprotective activity through suppression of NLRP1 inflammasome in ischaemic stroke mice. Exp Ther Med 25: 8, 2022.
21. Pieroni A and Pachaly P: Isolation and structure elucidation of ligustroflavone, a new apigenin triglycoside from the leaves of *Ligustrum* vulgare L. Pharmazie 55: 78-80, 2000.
22. MacArthur Clark JA and Sun D: Guidelines for the ethical review of laboratory animal welfare People's Republic of China national standard GB/T 35892-2018 [Issued 6 February 2018 Effective from 1 September 2018]. Animal Model Exp Med 3: 103-113, 2020.
23. Yang Y, Cai F, Zhou N, Liu S, Wang P, Zhang S, Zhang Y, Zhang A, Jia Z and Huang S: Dimethyl fumarate prevents ferroptosis to attenuate acute kidney injury by acting on NRF2. Clin Transl Med 11: e382, 2021.
24. Song J, Sheng J, Lei J, Gan W and Yang Y: Mitochondrial targeted antioxidant SKQ1 ameliorates acute kidney injury by inhibiting ferroptosis. Oxid Med Cell Longev 2022: 2223957, 2022.
25. Livak KJ and Schmittgen TD: Analysis of relative gene expression data using real-time quantitative PCR and the 2(-Delta Delta C(T)) method. Methods 25: 402-408, 2001.
26. Zilka O, Shah R, Li B, Friedmann Angeli JP, Griesser M, Conrad M and Pratt DA: On the mechanism of cytoprotection by ferrostatin-1 and liproxstatin-1 and the role of lipid peroxidation in ferroptotic cell death. ACS Cent Sci 3: 232-243, 2017.
27. Martinez Molina D, Jafari R, Ignatushchenko M, Seki T, Larsson EA, Dan C, Sreekumar L, Cao Y and Nordlund P: Monitoring drug target engagement in cells and tissues using the cellular thermal shift assay. Science 341: 84-87, 2013.
28. Bogen SA, Dabbs DJ, Miller KD, Nielsen S, Parry SC, Szabolcs MJ, t'Hart N, Taylor CR and Torlakovic EE: A consortium for analytic standardization in immunohistochemistry. Arch Pathol Lab Med 147: 584-590, 2022.
29. Trott O and Olson AJ: AutoDock Vina: Improving the speed and accuracy of docking with a new scoring function, efficient optimization, and multithreading. J Comput Chem 31: 455-461, 2010.
30. Zhang L, Chen F, Dong J, Wang R, Bi G, Xu D, Zhang Y, Deng Y, Lin W, Yang Z and Cao W: HDAC3 aberration-incurred GPX4 suppression drives renal ferroptosis and AKI-CKD progression. Redox Biol 68: 102939, 2023.
31. Wang Y, Zhang M, Bi R, Su Y, Quan F, Lin Y, Yue C, Cui X, Zhao Q, Liu S, *et al*: ACSL4 deficiency confers protection against ferroptosis-mediated acute kidney injury. Redox Biol 51: 102262, 2022.
32. Ranea-Robles P, Launay N, Ruiz M, Calingasan NY, Dumont M, Naudí A, Portero-Otín M, Pamplona R, Ferrer I, Beal MF, *et al*: Aberrant regulation of the GSK-3β/NRF2 axis unveils a novel therapy for adrenoleukodystrophy. EMBO Mol Med 10: e8604, 2018.
33. Jamadar A and Rao R: Glycogen synthase kinase-3 signaling in acute kidney injury. Nephron 144: 609-612, 2020.
34. Sohaney R, Yin H, Shahinian V, Saran R, Burrows NR, Pavkov ME, Banerjee T, Hsu CY, Powe N, Steffick D, *et al*: In-hospital and 1-year mortality trends in a national cohort of US veterans with acute kidney injury. Clin J Am Soc Nephrol 17: 184-193, 2022.
35. Coca SG, Singanamala S and Parikh CR: Chronic kidney disease after acute kidney injury: A systematic review and meta-analysis. Kidney Int 81: 442-448, 2012.
36. Turgut F, Awad AS and Abdel-Rahman EM: Acute kidney injury: Medical causes and pathogenesis. J Clin Med 12: 375, 2023.
37. Sanz AB, Sanchez-Niño MD, Ramos AM and Ortiz A: Regulated cell death pathways in kidney disease. Nat Rev Nephrol 19: 281-299, 2023.
38. Tonnus W, Meyer C, Steinebach C, Belavgeni A, von Mässenhausen A, Gonzalez NZ, Maremonti F, Gembardt F, Himmerkus N, Latk M, *et al*: Dysfunction of the key ferroptosis-surveilling systems hypersensitizes mice to tubular necrosis during acute kidney injury. Nat Commun 12: 4402, 2021.
39. Chen GL, Fan MX, Wu JL, Li N and Guo MQ: Antioxidant and anti-inflammatory properties of flavonoids from lotus plumule. Food Chem 277: 706-712, 2019.
40. Feng YD, Ye W, Tian W, Meng JR, Zhang M, Sun Y, Zhang HN, Wang SJ, Wu KH, Liu CX, *et al*: Old targets, new strategy: Apigenin-7-O-β-d-(-6''-p-coumaroyl)-glucopyranoside prevents endothelial ferroptosis and alleviates intestinal ischemia-reperfusion injury through HO-1 and MAO-B inhibition. Free Radic Biol Med 184: 74-88, 2022.
41. Han XH, Hong SS, Hwang JS, Lee MK, Hwang BY and Ro JS: Monoamine oxidase inhibitory components from Cayratia japonica. Arch Pharm Res 30: 13-17, 2007.
42. Jang DS, Lee YM, Jeong IH and Kim JS: Constituents of the flowers of Platycodon grandiflorum with inhibitory activity on advanced glycation end products and rat lens aldose reductase in vitro. Arch Pharm Res 33: 875-880, 2010.
43. Wang X, Chen T, Chen S, Zhang J, Cai L, Liu C, Zhang Y, Wu X, Li N, Ma Z, *et al*: STING aggravates ferroptosis-dependent myocardial ischemia-reperfusion injury by targeting GPX4 for autophagic degradation. Signal Transduct Target Ther 10: 136, 2025.
44. Jiang X, Stockwell BR and Conrad M: Ferroptosis: Mechanisms, biology and role in disease. Nat Rev Mol Cell Biol 22: 266-282, 2021.
45. Zeng Y, Xiong L, Tang H, Chen L, Yu Q, Li L, Chen F, Li L, Zheng Y, Sun J, *et al*: Norboldine improves cognitive impairment and pathological features in Alzheimer's disease by activating AMPK/GSK3β/Nrf2 signaling pathway. J Ethnopharmacol 333: 118498, 2024.

46. Song M, Zhang S, Yu W and Fan X: Gomisin N rescues cognitive impairment of Alzheimer's disease by targeting GSK3β and activating Nrf2 signaling pathway. Phytomedicine 132: 155811, 2024.
47. Lu C, Xu C, Li S, Ni H and Yang J: Liraglutide and GLP-1(9-37) alleviated hepatic ischemia-reperfusion injury by inhibiting ferroptosis via GSK3β/Nrf2 pathway and SMAD159/Hepcidin/FTH pathway. Redox Biol 79: 103468, 2025.
48. Fan G, Huang L, Wang M, Kuang H, Li Y and Yang X: GPAT3 deficiency attenuates corticosterone-caused hepatic steatosis and oxidative stress through GSK3β/Nrf2 signals. Biochim Biophys Acta Mol Basis Dis 1870: 167007, 2024.
49. Lv M, Cai Y, Hou W, Peng K, Xu K, Lu C, Yu W, Zhang W and Liu L: The C5AR1/TNFSF13B axis alleviates osteoarthritis by activating the PI3K/Akt/GSK3β/Nrf2/HO-1 pathway to inhibit ferroptosis. Exp Cell Res 441: 114195, 2024.
50. Chen P, Huo X, Liu W, Li K, Sun Z and Tian J: Apigenin exhibits anti-inflammatory effects in LPS-stimulated BV2 microglia through activating GSK3β/Nrf2 signaling pathway. Immunopharmacol Immunotoxicol 42: 9-16, 2020.
51. Wang L, Ouyang S, Li B, Wu H and Wang F: GSK-3β manipulates ferroptosis sensitivity by dominating iron homeostasis. Cell Death Discov 7: 334, 2021.
52. Feng X, Guan W, Zhao Y, Wang C, Song M, Yao Y, Yang T and Fan H: Dexmedetomidine ameliorates lipopolysaccharide-induced acute kidney injury in rats by inhibiting inflammation and oxidative stress via the GSK-3β/Nrf2 signaling pathway. J Cell Physiol 234: 18994-19009, 2019.
53. Cai YT, Li Z, Wang YY, Li C and Ma QY: A novel GSK3β inhibitor 5n attenuates acute kidney injury. Heliyon 10: e29159, 2024.
54. Lu M, Wang P, Qiao Y, Jiang C, Ge Y, Flickinger B, Malhotra DK, Dworkin LD, Liu Z and Gong R: GSK3β-mediated Keap1-independent regulation of Nrf2 antioxidant response: A molecular rheostat of acute kidney injury to chronic kidney disease transition. Redox Biol 26: 101275, 2019.

Copyright © 2026 Song et al. This work is licensed under a Creative Commons Attribution-NonCommercial-NoDerivatives 4.0 International (CC BY-NC-ND 4.0) License.